Background: Cryptogenic multifocal ulcerous stenosing enteritis (CMUSE) is a rare illness characterized by multiple strictures and shallow ulcers of the small bowel. Even though diagnostic criteria have been described, further ellucidation is needed on therapeutic interventions and potential discriminating factors between CMUSE and other more common causes of intestinal ulcerations, including Crohn's disease.

Aim: The purpose of this article is to report the clinical, CT, and MR enterography characteristics of confirmed cases of CMUSE.

Materials and Methods: Retrospective review of electronic medical records identified 33 patients considered for a diagnosis CMUSE. Diagnosis was confirmed if all requirements of the previously published diagnostic criteria for CMUSE were met. Patients were excluded if they had less than one year follow-up or incomplete clinical data. Two GI radiologists reviewed all CT and MR enterography (CTE/MRE) exams in consensus of confirmed patients to characterize the cross sectional imaging features.

Results: CMUSE was confirmed in 9 patients (27%) and 24 patients (73%) had a confirmed alternative diagnosis. Crohn's disease (CD) (30%, n=7) and drug-induced enteropathy (30%, n=7) were the most frequent alternative. Male gender (66.7% vs. 25%, p=0.04) and clinical manifestation of anemia at presentation were more commonly observed on CMUSE-confirmed cases (66.7% vs. 4.2%, p=0.005) when compared to patients with non-CMUSE diagnosis, in which abdominal pain was the most common presenting symptom (44.5% vs 87.5%, p=0.02). Multiple (100%) and circumferential (75%) ulcers with restricted mucosal involvement (55.6%) were major features at endoscopy and pathology. Most common treatments were corticosteroids (78%) or surgical resection (55.6%), with 33% receiving biologics. Disease recurrence after first treatment occurred in the majority (88.9%) after a median time of 6 months (Table 1).

9 CTE and 1 MRE of 8 confirmed cases images were analyzed (Table 2). Major imaging features included multiple (≥ 5; 88%; 7/8), short (< 2 cm; 100%; 8/8) circumferential (100%;8/8) strictures with moderate wall thickening (6–9 cm), and stratified hyper enhancement (100%; 8/8) located in the ileum (100%; 8/8). Median proximal small bowel dilation was 2.95 cm (2.5–4.1 cm). Less common findings included: mesenteric adenopathy (50%; 4/8), increased mesenteric edema/ascites (38%; 3/8), mesenteric vascularity (25%; 2/8), colon inflammation (13%; 1/8), and decreased small bowel fold pattern (13%; 1/8). No patients with confirmed CMUSE cases demonstrated penetrating disease (e.g., abscess, fistula).

Conclusion: CMUSE is rare cause of small bowel strictures with overlapping clinical and imaging features of more common etiologies such as Crohn's Disease and NSAID enteropathy that need to be excluded through a multidisciplinary approach to confirm the diagnosis.

Table 1. Baseline, Clinical and Treatment Characteristics of Confirmed CMUSE Patients

Characteristics, n (%) or median (IQR)		CMUSE Confirmed Patients (N = 9)
Age at diagnosis (years)		66 (44-70)
Female gender		3 (33.3%)
BMI at diagnosis (kg/m2)		25.4 (18.7-27.5)
Duration of Symptoms prior to diagnosis (months)		33 (24-103)
Time of Follow-up (months)		95 (42.5114.5)
History at First Presentation	Iron Deficiency Anemia	7 (77.8%)
	Abdominal Pain	4 (44.4%)
	Diarrhea	1 (11.1%)
	Weight Loss	3 (33.3%)
	Prior Obstructions	2 (22.2%)
	NSAID Use	3 (33.3%)
	Concomitant Celiac Disease	1 (11.1%)
	Gastric or Colon Involvement	1 (11.1%)
	Extra-intestinal Manifestations	0
Laboratory Findings at Diagnosis	Hemoglobin (g/dL)	11.3 (9.5-12.4)
	C-Reactive Protein (mg/L)	12 (3-24.0)
	Positive ANA	2/4 (50%)
	Positive ASCA or ANCA	1/6 (16.7%)
Diagnostic Modalities for Strictures	CT or MR Enterography	9 (100%)
	Enteroscopy	9 (100%)
	Capsule Endoscopy	(44.4%)
Endoscopic Characteristics	Multiple Strictures	9 (100%)
	Demarcated Ulcers	8 (88.9%)
	Circumferential Ulcers	7 (77.8%)
Histologic Characteristics	Mucosal Involvement	5 (55.6%)
	Submucosal Involvement	4 (44.4%)
	Lymphocyte predominant	4/5 (80%)
Treatment	Corticosteroids	7 (77.8%)
	Immunomodulator (MTX or AZA)	2 (22.5%)
	Biologic Therapy	3 (33.3%)
	Surgery	5 (55.6%)
	Endoscopic Dilation	3 (33.3%)
Outcomes	Median Time to First Recurrence (months)	5 (2-16.5)
	Refractory to First Treatment	8 (88.9%)
	Refractory to Steroids	6/7 (85.7%)
	Refractory To Surgery	2/5 (40%)
	Hospitalization for Obstruction During Disease Course	6 (66.7%)
	Mortality	2 (22.2%)

Legend: ANA, anti-nuclear antibody; ANCA, anti-neutrophil cytoplasmic antibody; ASCA, Anti-Saccharomyces cerevisiae *antibodies*, AZA, azathioprine; BMI, body mass index; CT, computed tomography; IQR, interquartile range; MRI, magnetic resonance imaging; MTX, methotrexate.

Table 2. CTE/MRE Image Analysis for confirmed CMUSE Patients

Stricture Imaging Features n=8 (%)		
Location	*Ileum*	100 (8/8)
	Jejunum	50 (4/8)
# per patient	*1*	13 (1/8)
	2-5	13 (1/8)
	5-10	38 (3/8)
	>10	50 (4/8)
Length	*<5 mm (web)*	50 (4/8)
	< 2cm (diaphragm)	100 (8/8)
	2-5 cm	50 (4/8)
	>5 cm	25 (2/8)
Morphology	*Circumferential*	100 (8/8)
	Asymmetric	50 (4/8)
SB Fold Pattern	*Normal*	88 (7/8)
	Decreased	13 (1/8)
Enhancement & DWI Characteristics	*Increased Stratified Pattern*	100 (8/8)
	Increased DWI	13 (1/8)
Measurements	*Prox. SB Dilation (cm) median (range)*	2.95 (2.5-4.1)
	Max Bowel Wall Thickness (mm) median (range)	6.5 (6-9)
% SB Involvement	*< 25%*	38(3/8)
	25-50%	50 (4/8)
	>75%	13 (1/8)

Extra-enteric Features n=8 (%)		
Mesenteric Vascularity	*Normal*	75 (6/8)
	Increased	25 (2/8)
Perienteric Changes	*Ascites*	25 (2/8)
	Edema	13 (1/8)
Mesenteric Lymph Nodes	*Numerous*	100 (8/8)
	Non-Enlarged	50 (4/8)
	Enlarged	50 (4/8)
Colon Abnormality	*Absent*	88 (7/8)
	Present	13 (1/8)

IDENTIFYING RELEVANT PATHWAYS AND BIOMARKERS IN CROHN'S DISEASE USING CONTEXTUALIZED METABOLIC NETWORK MODEL

Brooklyn McGrew, Aman Shrivastava, Philip Fernandes, Lubaina Ehsan, Yash Sharma, Dawson Payne, Lillian Dillard, Deborah Powers, Jason Papin, Richard Kellermayer, Anne Griffiths, Anthony Otley, Ashish Patel, Barbara Kirschner, David Mack, David Ziring, Dedrick Moulton, James Markowitz, Jason Shapiro, Jeffrey Hyams, Jennifer Dotson, Joel Rosh, Joshua Noe, Maria Oliva-Hemker, Marian Pfefferkorn, Melvin Heyman, Ajay Gulati, Robert Baldassano, Sandra Kim, Scott Snapper, Shervin Rabizadeh, Stanley Cohen, Stephen Guthery, Susan Baker, Tom Walters, Yael Haberman, Sean Moore, Subra Kugathasan, Lee Denson, Sana Syed

Background: Candidate markers for Crohn's Disease (CD) may be identified via gene expression-based construction of metabolic networks (MN). These can computationally describe gene-protein-reaction associations for entire tissues and also predict the flux of reactions (rate of turnover of specific molecules via a metabolic pathway). Recon3D is the most comprehensive human MN to date. We used publicly available CD transcriptomic data along with Recon3D to identify metabolites as potential diagnostic and prognostic biomarkers.

Methods: Terminal ileal gene expression profiles (36,372 genes; 218 CD. 42 controls) from the RISK cohort (Risk Stratification and Identification of Immunogenetic and Microbial Markers of Rapid Disease Progression in Children with Crohn's Disease) and their transcriptomic abundances were used. Recon3D was pruned to only include RISK dataset transcripts which determined metabolic reaction linkage with transcriptionally active genes. Flux balance analysis (FBA) was then run using RiPTiDe with context specific transcriptomic data to further constrain genes **(Figure 1)**. RiPTiDe was independently run on transcriptomic data from both CD and controls. From the pruned and constricted MN obtained, reactions were extracted for further analysis.

Results: After applying the necessary constraints to modify Recon3D, 527 CD and 537 control reactions were obtained. Reaction comparison with a publicly available list of healthy small intestinal epithelial reactions (n=1282) showed an overlap of 80 CD and 84 control reactions. These were then further grouped based on their metabolic pathways. RiPTiDe identified context specific metabolic pathway activity without supervision and the percentage of forward, backward, and balanced reactions for each metabolic pathway **(Figure 2)**. The metabolite concentrations in the small intestine was altered among CD patients. Notably, the citric acid cycle and malate-aspartate shuttle were affected, highlighting changes in mitochondrial metabolic pathways. This is illustrated by changes in the number of reactions at equilibrium between CD and control.

Conclusions: The results are relevant as cytosolic acetyl-CoA is needed for fatty acid synthesis and is obtained by removing citrate from the citric acid cycle. An intermediate removal from the cycle has significant cataplerotic effects. The malate-aspartate shuttle also allows electrons to move across the impermeable membrane

in the mitochondria (fatty acid synthesis location). These findings are reported by previously published studies where gene expression for fatty acid synthesis is altered in CD patients along with mitochondrial metabolic pathway changes, resulting in altered cell homeostasis. In-depth analysis is currently underway with our work supporting the utility of potential metabolic biomarkers for CD diagnosis, management and improved care.

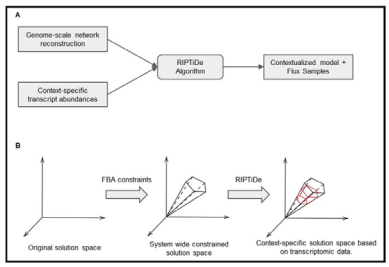

Figure 1: (A) A schematic representation of the computation process to identify a contextualized metabolic model using the RIPTiDe algorithm. **(B)** Visual representation of the RIPTiDe algorithm on the solution space, first showing the effect of the system wide constraints followed by the red box highlighting constrained solutions based on transcriptomic data.

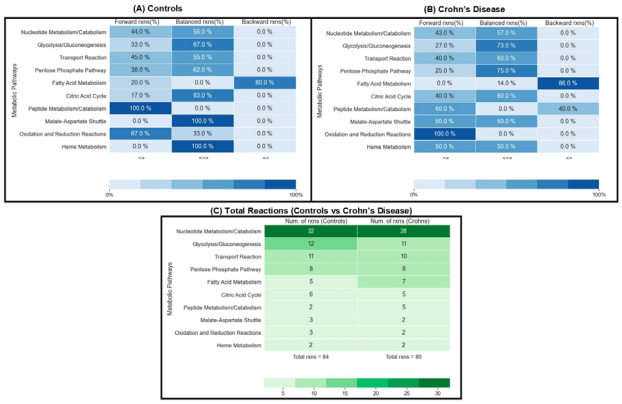

Figure 2: RIPTiDe identified context-specific metabolic pathways active in **(A) Control group** and **(B) pediatric Crohn's disease**, using corresponding transcriptomic data. **(C)** highlights the total reactions in each metabolic pathway for both Controls and Crohn's Disease. ***Note:*** For **(A)** and **(B)**, a darker color represents a higher percentage of reactions in that category. For **(C)** a darker color represents a higher number of reactions in the corresponding category.
Key: rxns - Reactions.

MACHINE LEARNING FOR CROHN'S DISEASE PHENOTYPE MODELING USING BIOPSY IMAGES

Sana Syed, Saurav Sengupta, Lubaina Ehsan, Erin Bonkowski, Christopher Moskaluk, Anne Griffiths, Anthony Otley, Ashish Patel, Barbara Kirschner, David Mack, David Ziring, Dedrick Moulton, James Markowitz, Jason Shapiro, Jeffrey Hyams, Jennifer Dotson, Joel Rosh, Joshua Noe, Maria Oliva-Hemker, Marian Pfefferkorn, Melvin Heyman, Ajay Gulati, Richard Kellermayer, Robert Baldassano, Sandra Kim, Scott Snapper, Shervin Rabizadeh, Stanley Cohen, Stephen Guthery, Subra Kugathasan, Susan Baker, Tom Walters, Lee Denson

Background: Predicting Crohn's disease (CD) phenotype development has proven challenging due to difficulties in biopsy image interpretation of histologically similar yet biologically distinct phenotypes. At initial diagnosis, mostly CD patients are classified as B1 (inflammatory behavior), they typically either retain B1 phenotype or develop more complicated B2 (stricturing), B3 (internal penetrating), or B2/B3 phenotypes (defined by Montreal Classification). Prediction of phenotype development based on baseline biopsies can radically improve our clinical care by altering disease management. Biopsy-based image analysis via Convolutional Neural Networks (CNNs) has been successful in cancer detection, but investigation into its utility for CD phenotypes is lacking. We applied a machine learning CNN model to classify CD phenotypes and histologically normal ileal controls.

Methods: Baseline hematoxylin & eosin (H&E) stained ileal biopsy slides were obtained from the Cincinnati Children's Hospital Medical Center's RISK validation sub cohort. At University of Virginia, biopsy slides were digitized, and a ResNet101 CNN model was trained. High resolution images were patched into 1000x1000 pixels with a 50% overlap and then resized to 256x256 pixels for training (80-20 split was kept between training and testing sets to ensure same patient patches were not mixed). Gradient Weighted Activating Mappings (GradCAMs) were used to visualize the model's decision making process.

Results: We initially trained the model for CD vs. controls where it achieved 97% accuracy in detecting controls. We further trained it for classifying CD phenotypes (n=16 B1, n=16 B2, n=4 B3, n=13 B2/B3; phenotype decision at 5 year). It displayed a higher accuracy in detecting B2 (85%) while there were overlaps in the detection of other phenotypes (Figure 1). For B2, Grad-CAM heatmaps highlighted central pink areas within the lamina propria as the model's regions of interests which were present when other phenotypes were misclassified as B2 (Figure 2). Conclusions: Here we highlight the potential utility of a machine learning image analysis model for describing CD phenotypes using H&E stained biopsies. Previous studies have shown B2 to be associated with increased activation for extracellular matrix genes (connective tissue component). Our GradCAM results support this finding as the pink central areas utilized by the model for classifying B2 could be connective tissue. Further confirmation via molecular phenotyping including Sirius Red immunohistochemistry is underway. Our work supports prediction of CD phenotypes using baseline biopsies at diagnosis and has potential to influence individualized care for children with CD.

Figure 1: Model classification accuracies for CD phenotypes

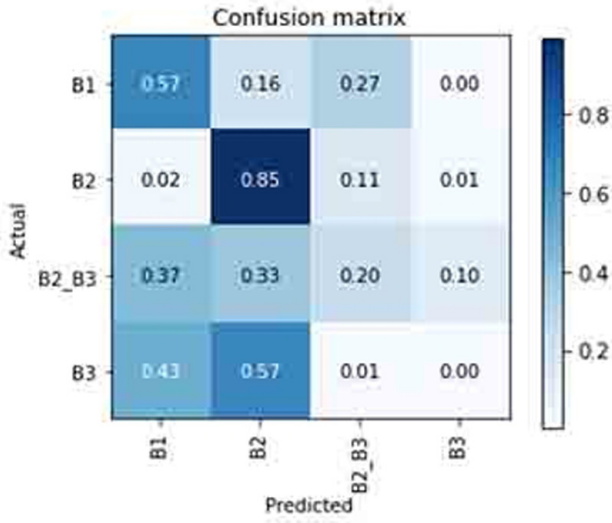

Figure 2: Grad-CAMs for B2 (yellow shows regions of interest for the model). Biopsy images shown are from a patient diagnosed with: A-B2 classified as B2 by the model; B-B1 classified as B2; C-B3 classified as B2